DISCLAIMER

CONF-930202--5

PNL-SA--21085

DE93 008924

MATERIALS CHARACTERIZATION OF CERMET ANODES TESTED IN A PILOT CELL

T. R. Alcorn
N. E. Richards
D. M. Strachan
A. T. Tabereaux
C. F. Windisch, Jr.
C. H. Henager, Jr.

February 1993

Presented at the
Minerals, Metals, and
Materials Society
122nd Annual Meeting
February 21-25, 1993
Denver, Colorado

Prepared for
the U.S. Department of Energy
under Contract DE-AC06-76RLO 1830

MASTER

Pacific Northwest Laboratory
Richland, Washington 99352

DISTRIBUTION OF THIS DOCUMENT IS UNLIMITED

MATERIALS CHARACTERIZATION OF CERMET ANODES TESTED IN A PILOT CELL

C. F. Windisch Jr., D. M. Strachan and C. H. Henager Jr.
Pacific Northwest Laboratory[a]
Richland, WA 99352

T. R. Alcorn, A. T. Tabereaux and N. E. Richards
Manufacturing Technology Laboratory
Reynolds Metals Company
3326 East Second Street
Muscle Shoals, AL 35661-1258

Abstract

Cermet anodes were evaluated as nonconsumable substitutes for carbon anodes using a pilot scale reduction cell at the Reynolds Manufacturing Technology Laboratory. After pilot cell testing, the anodes were subjected to extensive materials characterization and physical properties measurements at the Pacific Northwest Laboratory. Significant changes in the composition of the cermet anodes were observed including the growth of a reaction layer and penetration of electrolyte deep into the cermet matrix. Fracture strength and toughness were measured as a function of temperature and the ductile-brittle transition was reduced by 500°C following pilot cell testing. These results imply difficulties with both the anode material and the control of operating conditions in the pilot cell, and suggest that additional development work be performed before the cermet anodes are used in commercial reduction cells. The results also highlight specific fabrication and operational considerations that should be addressed in future testing.

Introduction

The Inert Electrodes Program is being conducted at the Pacific Northwest Laboratory (PNL) for the U. S. Department of Energy (DOE), Office of Industrial Processes (OIP). The purpose of the program is to develop long-lasting, energy-efficient anodes, and ancillary equipment for Hall-Heroult cells used to produce aluminum metal. Emphasis has been placed on testing anodes made from a ceramic/metal composite consisting of NiO and nickel ferrite and a Cu-Ni metal phase. Anodes of this type were first developed by Alcoa Laboratories (Alcoa Center, PA) in a program also sponsored by DOE (1). Laboratory tests (1,2) have shown that this composition corrodes at a low enough rate to make it an attractive alternative to the consumable carbon anodes currently used in commercial smelting operations. Before aluminum companies would consider using the cermet anodes, however, it was necessary to demonstrate success in a scaled-up operation. In particular, acceptable performance had to be shown in a larger, self heated cell. Toward this end, Reynolds Metals Company (RMC) was subcontracted by PNL to use the "pilot cell" at the Manufacturing Technology Laboratory (MTL) in Muscle Shoals, AL. The pilot cell was subsequently modified to test cermet anodes. A preliminary "prototype anode test" was also performed by RMC and PNL in a large laboratory cell at the MTL in March 1989 to determine certain operating conditions for the cermet anodes before running the pilot cell test(3,4).

The pilot cell test was started on August 1, 1991. Between August 1 and August 30, PNL and RMC assisted each other in the evaluation of 13 cermet anodes that were manufactured by Ceramic Magnetics, Inc. (CMI, Fairfield, NJ). Operational difficulties were encountered during the test as discussed in a separate paper in this volume (5) and the pilot cell test procedures had to be modified severely. Nevertheless, cermet anodes were tested in the pilot cell for as long as 314 h (13.1 days) under conditions close to those in an industrial environment. After the test was completed, the anodes were returned to PNL for various "post-test" analyses. The results of these analyses are discussed in this paper.

It is important to recognize that the primary objective of the pilot cell test was *to evaluate the "inertness" of cermet anodes as nonconsumable substitutes for carbon in a pilot reduction cell.* If the material could be shown to corrode or wear at acceptably low rates in this test, it was hoped that industry would become sufficiently interested in the material and the inert-anode alternative to proceed with the next step in transferring the technology to commercial cells.

Discussion

Anode Construction

A set of 13 cermet anodes were produced at CMI for use by RMC and PNL in the pilot cell test.[b] The powder from which these anodes were produced was also made at CMI. This section covers some of the more important issues associated with both the fabrication of the powder and the cermet anodes themselves.

Ceramic Powder. A large, approximately 1000-kg, batch of the ceramic powder was prepared from hematite (Fe_2O_3, Pfizer Pigments, Inc., Easton, NJ) and high purity, green nickel oxide (NiO, Novamet, Wyckoff, NJ). The powder preparation involved blending the raw materials, milling, calcining, and then spray drying. The initial conditions for each step were discussed

[a] Operated for the U.S. Department of Energy by Battelle Memorial Institute under Contract DE-AC06-76RL 1830.

[b] Additional anodes were also made for subsequent evaluation by RMC and the Eltech Research Corporation (ERC) in a later phase of the pilot cell test (6).

previously (7); however, as indicated below, some of the procedures had to be modified at CMI to obtain powder with the desired properties. Small test batches of powder were therefore first prepared to determine the best procedures using the CMI facilities.

The starting materials were mixed wet (H_2O) in a steel ball mill for 2 h to 4 h, and then dried. Eight 50-kg batches of the powder were calcined at different conditions to attain a fully reacted and sinterable powder. Chemical analysis of the powder that served as the source for all of the calcining trials and the pilot cell anodes indicated the actual composition was very close to the targeted composition (46.5 w/o Fe_2O_3; 51.7 w/o NiO). For initial batches of the powder, the calcining was not performed at sufficiently high temperatures so that the main constituents were basically unreacted Fe_2O_3 and NiO. As the temperature and time at temperature were increased in later batches from 800°C for 2 h to 980°C for 6 h, the amount of these materials decreased in favor of the desired compound with nominal stoichiometry $NiFe_2O_4$.

One of the problems identified early in the program was the low consolidation pressures available at CMI. The maximum pressure that could be attained at CMI was 91 MPa (13 ksi). This is substantially lower than the 140 MPa (20 ksi) used in the laboratory studies at PNL. This low consolidation pressure led to a density approximately 0.1 $g \cdot cm^{-3}$ lower than obtained at the higher pressure, i.e. 6.1 $g \cdot cm^{-3}$. (It is worth noting that pellets made from earlier batches of the calcined powder containing significant amounts of Fe_2O_3 gave sintered densities close to 6.1 $g \cdot cm^{-3}$ when they were pressed at 140 MPa.)

Twenty-five-kilogram batches of powder were also spray dried. Early batches were spray dried to a particle size of 84 μm. It was noted in small test batches taken from each 25-kg batch that this powder did not blend well with Cu metal. The final 500-kg batch of powder prepared for the pilot cell anodes was spray dried to a particle size of 20 μm. The particle sizes of 20 μm and 50 μm represented the mean agglomerate size. The actual powder making up these agglomerates was probably in the range of 1 μm to 5 μm.

Since the batch size and furnace used in the trial calcinings was small, the conditions necessary to calcine the large 500-kg batch of powder for the pilot cell anodes were changed slightly. Whether this change or simply the difference in calcining a large batch of powder made the difference, the resulting powder had a trace of hematite and pellets made from the powder did not sinter to as high a density as the smaller batches of powder. The exact cause of this can only be speculated at this time, but one explanation is that portions of the powder were at the calcining temperature longer than other portions. This could possibly have been corrected by longer ball milling or use of a different furnace/furnace design so that uniform calcining occurred. Apparently, as a combined result of both the presence of the hematite and the lower consolidation pressure, the pilot cell anodes were about 0.2 $g \cdot cm^{-3}$ lower than those that had been fabricated at PNL as well as the prototype anode used in the large laboratory-scale test (4). The precise effects of this lower density on the performance of the anode material are not known, but they may have included an acceleration of some of the compositional and microstructural changes discussed later in this paper.

Anode Production. Using the spray dried powder described above mixed with 17 w/o Cu[c] metal (Alamo Supply Co., Houston, TX), a set of "preliminary" pilot cell anodes were fabricated. The powder was pressed at 91 MPa (13 ksi) and then sintered according to a 88 h schedule with a maximum temperature of 1200°C in a controlled atmosphere with 100 200 ppm O_2. The target anode dimensions shown in Figure 1 were obtained using a specially designed mold. To accommodate the Ni connector rod that was to be used to support the anodes and provide an electrical connection, a metal-rich core material had been developed (8) and is shown as the "inverted T" in Figure 1. This core was constructed of 50% cermet powder and 50% of an alloy that was 65% Cu and 35% Ni. The core material, when sintered in small laboratory-scale anodes, provided a good electrical bond between the Ni rod and the cermet anode body as well as a reasonable transition between the coefficient of thermal expansion of the cermet and the Ni rod. Unfortunately, this core caused the preliminary scaled-up anodes to crack during sintering so it was not used in the anodes actually made for the pilot cell test. The 13 anodes for the pilot cell test were made without the core material and the cermet was drilled and tapped directly to accommodate the Ni connector rod. Anodes made in this fashion contained no visible cracks after sintering. In addition, no cracks were found using ultrasonic methods on two of the anodes selected randomly from the batch of thirteen. The compositions of samples removed from sintered preliminary anodes were determined by wet lab analysis and found to be identical to the theoretical composition within experimental error (17 w/o Cu, 33.7 w/o Ni and 28.0 w/o Fe). The microstructure of a sample removed from a preliminary anode was also determined and is shown in Figure 2. As expected, the material contained three phases: NiO (dark gray), ferrite (light gray), and Cu-Ni alloy (white). However, some microstructural features appeared different in this sample than in anodes made

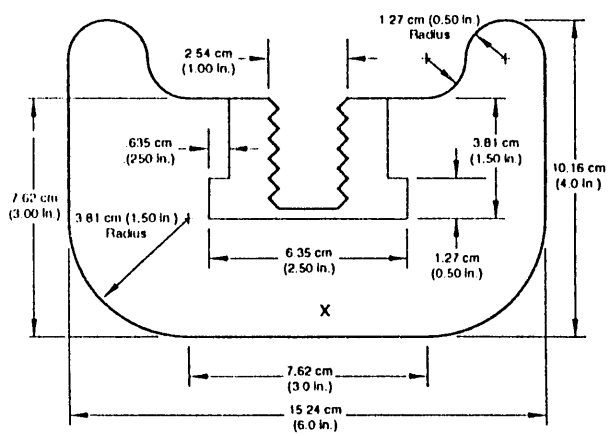

Figure 1: Nominal Dimensions of the Cermet Anode. (Inverted "T" around screw connection corresponds to a "core material" that was added in earlier configurations.)

[c] Although Cu metal was added during preparation of the anode, a Cu-Ni alloy is formed during sintering. The Ni component is believed to result from the reduction of some NiO by the residual organic sintering aids.

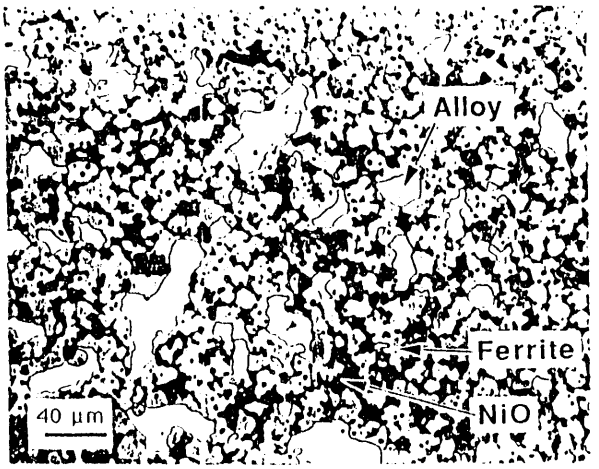

Figure 2: Optical Micrograph of Pilot Cell Anode Material Before Testing.

previously at PNL and Alcoa laboratories (1,7). For example, the material appeared to be more porous, probably because of the lower consolidation pressure used at CMI. Density measurements were also consistent with this conclusion as discussed below.

Pilot Cell Operation

Details of the pilot cell operation are given in a companion paper elsewhere in this volume (5). Two primary operational objectives for most of the duration of the pilot cell test were that the current density on any cermet anode not exceed 0.5 $A \cdot cm^{-2}$ and that alumina concentration be maintained as close as possible to saturation. These criteria were based on previous determinations of the least aggressive conditions for the cermet anodes (1,2,7,8). In reality, the alumina concentration varied significantly during the pilot cell test (5), and the current density varied dramatically around each anode. Nevertheless, the alumina concentration was usually kept reasonably high during the test at an average value of about 80% of saturation (despite the significant periodic excursions); and, as determined by local measurements of voltage drops, the current density did not exceed 0.5 $A \cdot cm^{-2}$ on any surface of the anodes, although on most surfaces it was probably much lower. Six cermet anodes were usually in operation at any one time in the configuration shown in Figure 3. The positions of each of the cermet anodes were labelled A through F, relative to the position of the large carbon anode, as shown in Figure 3. Individual anodes tested in each position were labelled separately[a] and are noted in Figure 3 along with the time of testing for each anode and the average current during that time.

A current of 90 A was calculated to correspond to a maximum current density of about 0.5 $A \cdot cm^{-2}$ on any surface based on early models of current flow. While the observed current flow in the pilot cell was

[a] The numbering scheme for the individual anodes is not obvious and reflects the changes in test procedures required because of operational problems (5).

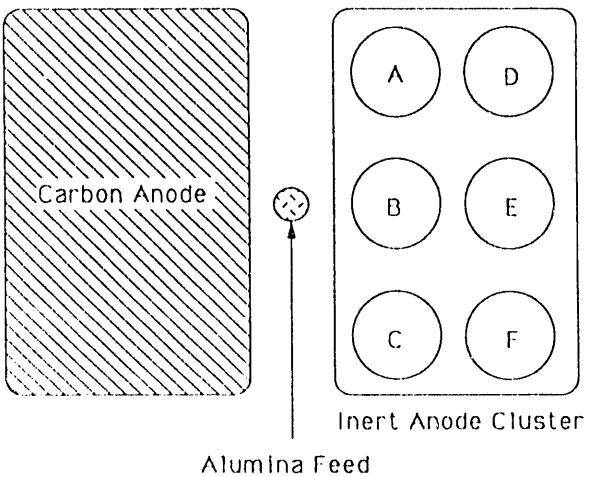

Position	Anodes	Time, h	Current, A
A	A1, E2*	193, 260	35, 74
B	Aux2, A2	181, 182	29, 51
C	C1, C2*	191, 260	51, 86
D	D1, D2	123, 279	82, 62
E	Aux1, E1*	313, 135	45, 72
F	F1, F2	314, 96	70, 41

Figure 3: Schematic of Anode Positions Showing Exchange Sequence and Test Conditions for Individual Anodes. (*Exposed to aggressive conditions.)

significantly different than anticipated from these early models, it turned out that the targeted current value was similar. By keeping the current to any one anode at 90 A or less, the current density on any surface of the anodes did not exceed 0.5 $A \cdot cm^{-2}$. In the case of anodes C2, E1, and E2, the anodes were deliberately subjected to higher currents at the very end of the pilot cell test to determine the effects of current density.

Anode Characterization

Twelve of the 13 anodes that were tested in the pilot cell were delivered to PNL for post-test analyses. (Anode B1 broke before it was inserted in the cell.) The results of these analyses are discussed in the following three sections concerning: 1) the overall appearance of the anodes and how this appearance and related dimensions changed upon testing, 2) the compositional and microstructural changes that occurred as a result of testing, and 3) the results of physical and mechanical properties measurements on the anodes.

Changes in Appearance and Dimensions. Figure 4 shows the cross section of part of the bottom edge of anode F1 after removal from the pilot cell. Anode F1 was tested for the longest period of time (314 h) under "normal" conditions, i.e. at less than or equal to 90 A and at high alumina concentrations. During operation with anode F1, the average current through anode F1 was 70 A and alumina concentration was 7.4 w/o where 8 w/o was approximately saturation for the typical conditions of this test. The anode was located in position F as indicated in Figure 3.

Figure 5 shows a similar view for anode C2 which was operated for a short period at the end of the test under "aggressive" conditions, i.e. when alumina concentration was dropped to about 20% of saturation and current was raised to twice the normal value (180 A). Anode C2 was in position C as shown in Figure 3.

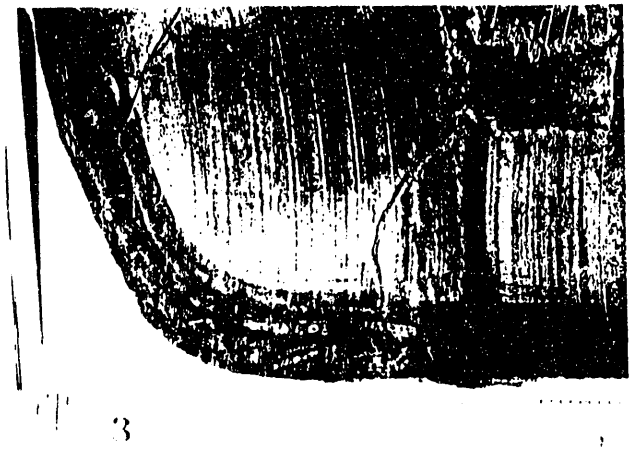

Figure 4: Cross Section of Bottom Edge of Cermet Anode F1.

Figure 5: Cross Section of Bottom Edge of Cermet Anode C2.

As illustrated in Figures 4 and 5, anodes that were in operation under the aggressive conditions of low alumina concentration and higher current density showed much more corrosion than those operated under normal conditions. Anode C2 exhibited very thick reaction product layers, generally gross and very irregular wear. In contrast, anodes tested under normal conditions did not appear to change much dimensionally, except for the growth of a reaction layer. Since the original shape of the anodes was largely preserved, this suggests the reaction layer formed under normal conditions occupied essentially the same volume as the unreacted material from which it formed.

The reaction layer was also thicker for anodes tested at longer times when other cell conditions were similar. The thickness of the reaction layer, measured at the center of anode diameter, is plotted in Figure 6 versus A·h for *all* of the pilot cell anodes. The data appear to be grouped into two regions. The anodes tested under aggressive conditions gave significantly higher reaction layer thicknesses (boxed area) than anodes tested under normal conditions. For anodes treated under normal conditions, the reaction layer thickness was about 13 mm after 314 h (13.1 days) of testing (anode F1); thicknesses for anodes treated under aggressive conditions were over 25 mm at much shorter times. The thicknesses of the reaction layers on the anodes treated under normal conditions appeared to follow a roughly linear trend with A·h as shown in Figure 6. The trend is not exact and estimated uncertainties fall short of explaining all the variances; however, given the varying conditions in the pilot cell test (5), it is likely that even these uncertainties were underestimated so that the linear approximation is not completely unfounded.

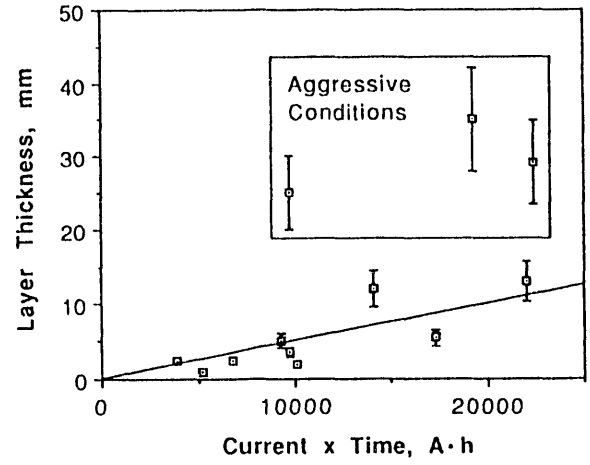

Figure 6: Variation of Reaction Layer Thickness with A·h for Cermet Anodes.

A linear fit to these data, excluding the severely corroded anodes and pinned to the origin to give no layer at the start of the test, gives a slope or layer growth rate equal to 5×10^{-4} mm·A^{-1}·h^{-1}, or 0.8 mm·day^{-1} for 70 A of current. Recognizing that this rate is appropriate for only those current densities close to the actual value at the bottom surface of these anodes (about 0.2 A·cm^{-2} from the calculations using data from voltage probes) and assuming linearity, this growth rate gives an extrapolated annual rate of 31 cm·yr^{-1} for a pilot cell-style anode operating at 70 A. This rate is inconsistent with extrapolated rates from earlier studies (1,2) and would be clearly unacceptable even if the properties of the reaction layer were not that detrimental. Of course, the extrapolation relies on the assumption of linearity

for up to a year's time. If the growth is not linear, and the thickness levels off after some time, the results may not be as unfavorable, provided the reaction layer imparts a sufficiently low resistance to the current path.

Changes in Microstructure and Composition. This section focuses on the microstructural and compositional analyses performed on anode F1, which was the anode tested for the longest time under normal operating conditions. A number of core sections were removed from anode F1 for analysis as shown in Figure 7. The samples labelled F1-B, F1-M and F1-T, removed from near the center of the diameter of the anode, encompassed regions from the very bottom surface of the anode, including the reaction layer discussed above, to the top surface of the anode. Based on voltage drop measurements made during the test, the bottom surface was estimated to have been subjected to a current density of approximately 0.2 $A \cdot cm^{-2}$.

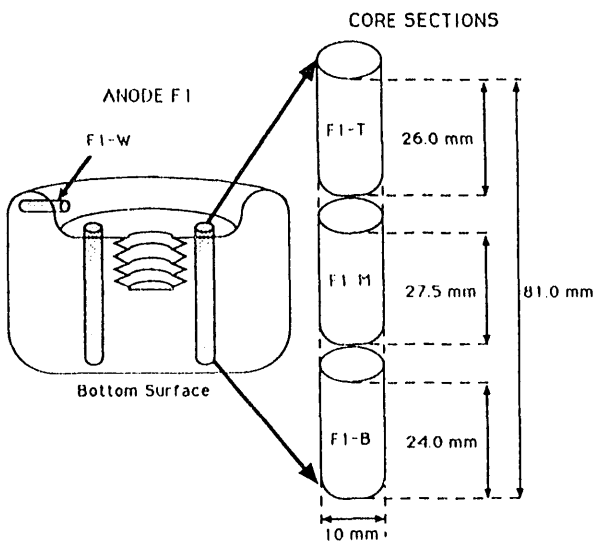

Figure 7: Core Sections Removed from Cermet Anodes for Analysis.

As shown in the scanning electron microscopy (SEM) backscattered image in Figure 8, sample F1-B contained essentially all of the "reaction layer" whose thickness variations were quantified earlier. The reaction layer in this region had an average thickness of 17.5 mm. The thickness varied somewhat in this region because it was near the beginning of the curvature of the bottom of the anode. As shown in Figure 8, the reaction layer was very complicated in structure and was composed of many sublayers. Energy dispersive x-ray spectroscopy (EDS) and x-ray diffraction (XRD) analyses indicated that the reaction layer was essentially devoid of metallic phase and the many sublayers were varied in composition. Copper, in particular, segregated into sublayers in the reaction zone. The Cu in this region was identified as mostly Cu_2O and Cu_xNi_yO phases using XRD. Other regions, in particular right at the surface, were severely depleted in Cu. In general, Fe was predominant in regions were Cu was absent and depleted in regions

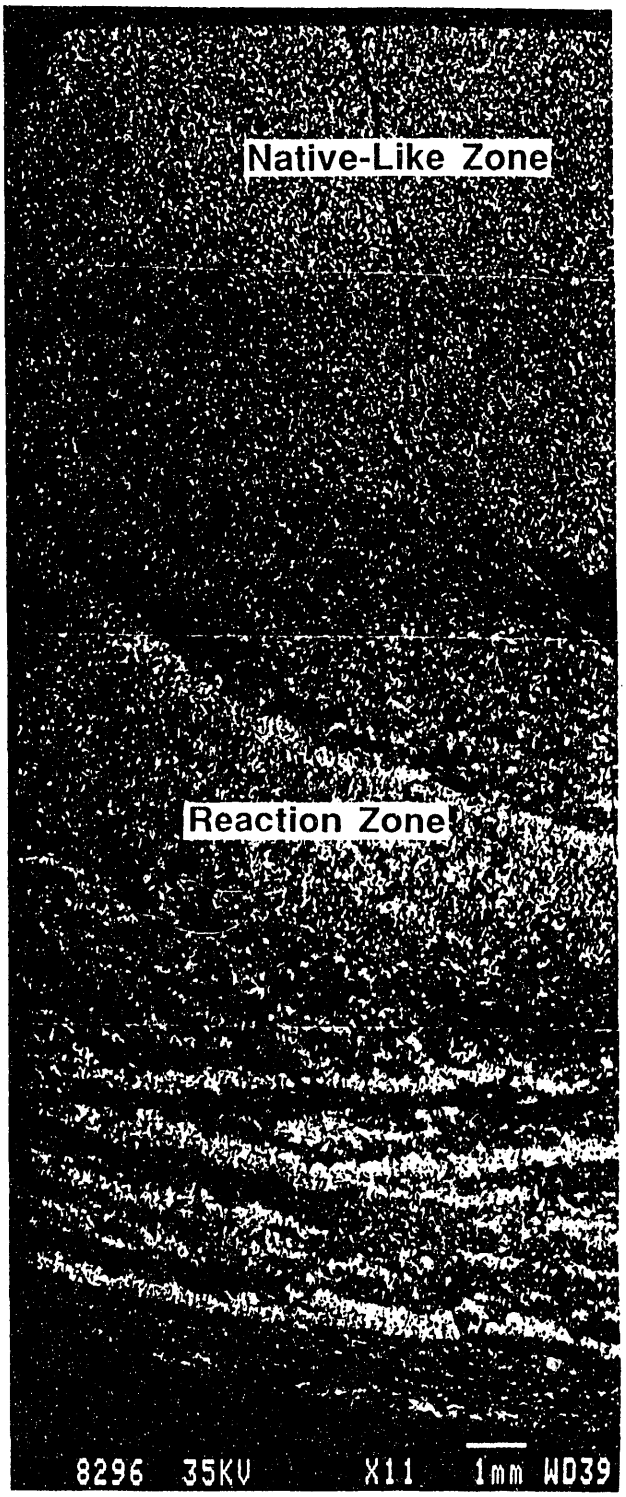

Figure 8: SEM Backscattered Image of Cross Section of Sample F1-B Removed from Anode F1.

where Cu content was high. Nickel was distributed more uniformly, but appeared to be more concentrated in regions high in Cu, particularly near the electrode surface. This is consistent with the formation of the Cu_xNi_yO compounds, that were identified with XRD.

Other phases in sample F1-B included Al-Ni-Fe compounds. The stoichiometry of some of these phases, determined using EDS, suggested they were formed by the replacement of Al for Fe to varying amounts in the original $NiFe_2O_4$ (ferrite) phase. This type of reaction was also observed in bench-scale tests (9) although to a much smaller extent. In general, the amount of substitution was the greatest right at the surface and decreased as a function of depth into the anode. In some cases, the phases may correspond to stoichiometric aluminates since Ni and Fe aluminates were detected in this region with XRD. As shown by the SEM image in Figure 9, the phases formed from the ferrite phase had a grain structure very different from the original. The grains in this region appear to have grown significantly and fused together forming one of the bands or sublayers in the lower-magnification image in Figure 8.

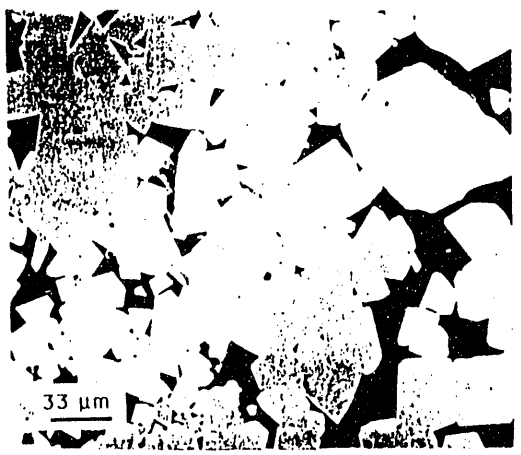

Figure 9: SEM Micrograph of Region in Reaction Layer Containing Consolidated Ferrite Phase.

Above the reaction layer in F1-B, the microstructure appears similar to the original or "native" microstructure as shown in Figure 8. This native microstructure extends up vertically through most of samples F1-M and F1-T. At the very top of F1-T, another, albeit much thinner, reaction layer was apparent. This layer was about 1.0 mm thick and was devoid of metallic phase like the thicker layer at the bottom surface.

The elemental dot map for Al for sample F1-B, shown in Figure 10, indicates that significant amounts of Al penetrated the anode. The penetration extended through the reaction layer and significantly into the native material. Some regions in F1-B were very rich in Al consistent with the formation of the Al-Ni-Fe phases. However, the penetration of the electrolyte also occurred into samples F1-M and F1-T as shown by the plot of the EDS signal intensity ratios in Figure 11. Significant amounts of fluorine were also detected in the interior of the anode. Results from EDS and XRD analyses indicated two types of compounds containing fluorine. As shown in Figure 12, one of

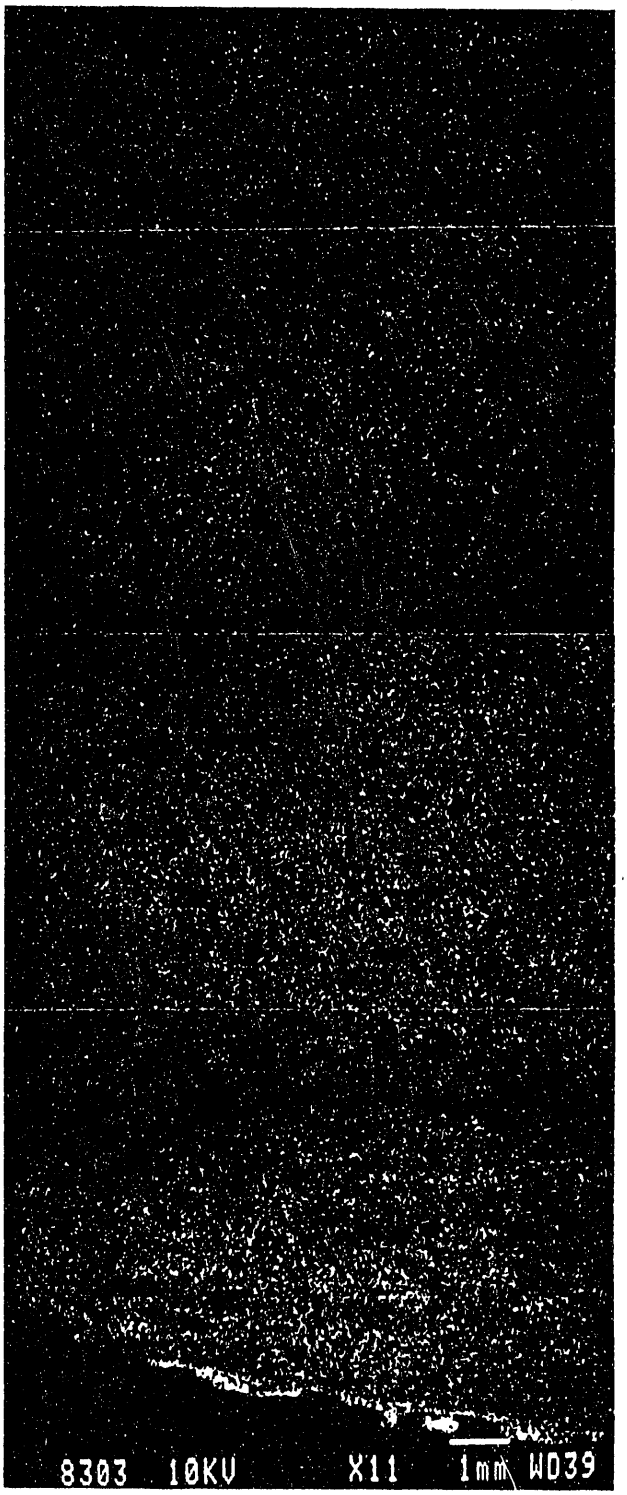

Figure 10: Elemental Dot Map for Al Showing Penetration into Sample F1-B. (Region shown is exactly the same region as shown in SEM image in Figure 8.)

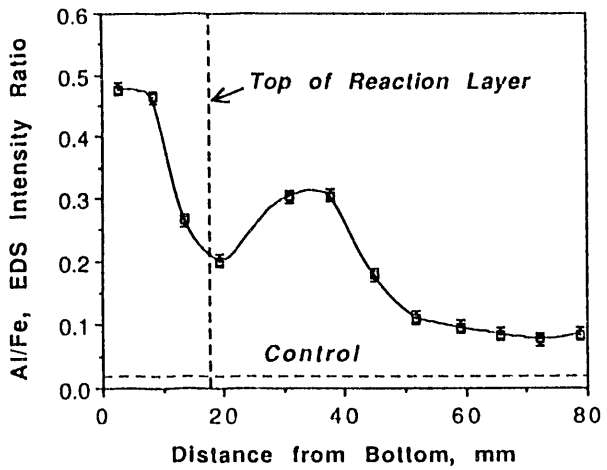

Figure 11: Variation of Al/Fe EDS Intensity Ratio as a Function of Distance from the Bottom of Anode F1.

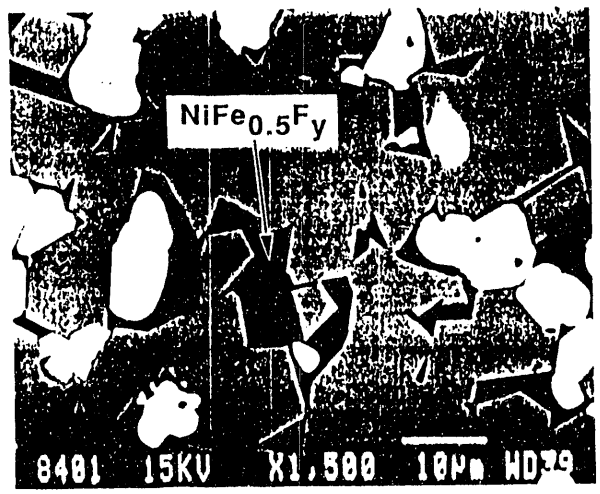

Figure 12: SEM Micrograph of Cross Section of Region in F1 Containing Ni-Fe Fluoride Phase.

these phases was detected using SEM on polished core samples. The phase was determined to be a Ni-Fe fluoride. It was found throughout the anode and typically contained more Fe at distances further from the bottom surface. XRD corroborated this finding by verifying the existence of NiF_2 in parts of the anode. Another fluoride phase was also identified using SEM, but only on fracture surfaces as shown in Figure 13. EDS analysis revealed this phase was an Al-containing fluoride compound (possibly containing oxide ions as well). The presence of an aluminum oxyfluoride species along grain boundaries was also detected with x-ray photoelectron spectroscopy (XPS) in previous studies at PNL (8). It seems reasonable that this species was the primary species migrating from the electrolyte into the interior of the anode. Transport apparently occurred along grain boundaries, although migration through pores is also possible.

Another important compositional change occurring in the pilot cell anodes concerned the metallic phase. As indicated previously, the phase was essentially absent from the reaction layer in sample F1-B. In the region of native microstructure just above the

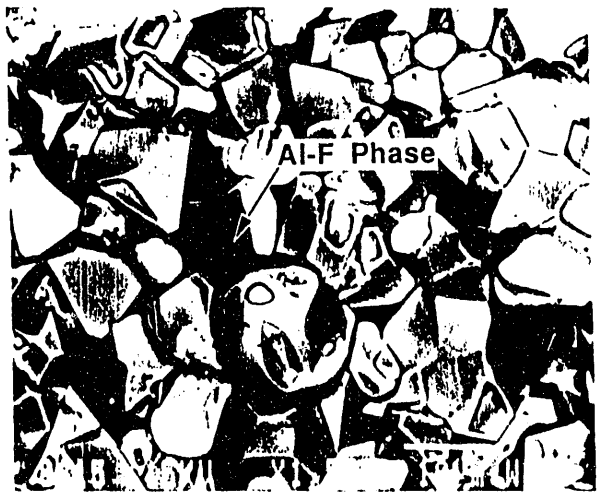

Figure 13: SEM Micrograph of Fracture Surface Showing Presence of Al-Fluoride Phase at the Grain Boundaries.

reaction layer in sample F1-B, however, the metallic phase was present and was composed of almost pure Cu. This is in contrast to the metallic phase in an unreacted anode which was an alloy with the nominal composition of 86 w/o Cu, 13 w/o Ni and 1 w/o Fe. The "refinement" of Cu in the metallic phase just above the reaction layer was observed in other studies on cermet anodes (4). As shown in Figure 14, the amount of Ni relative to Cu in the metallic phase rises from the very low value (almost pure Cu) right above the reaction layer to values close to an unreacted control anode (0.15) at further distances into the anode. At the top of the anode, where another reaction layer is present, the ratio again becomes low. The thickness of the Cu-enriched metallic zone seems to be related to the overall corrosion performance of the anode. For example, anode F1, which had a reaction layer about 13 mm thick on the average, showed a Cu-enriched metallic zone about 35 mm thick (Figure 14). In contrast, the prototype anode (4), which had a reaction layer about 3 mm thick, exhibited a Cu-

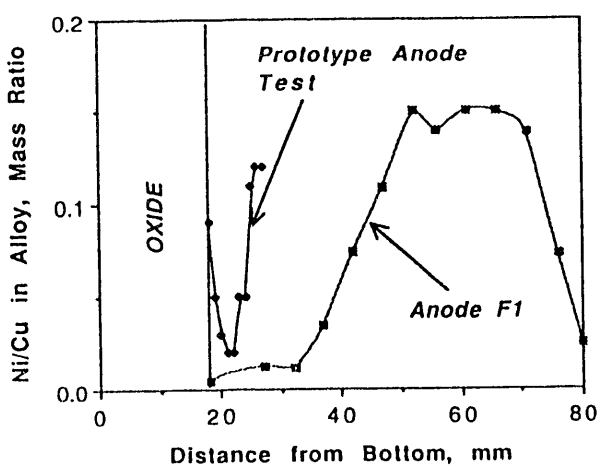

Figure 14: Ni/Cu Mass Ratio in the Alloy Phase as a Function of Distance from the Bottom of Tested Anodes.

enriched zone of only about 10 mm, as shown in Figure 14. The ratio of Cu-enriched zone thickness to reaction layer thickness is roughly 3, in both cases.

Changes in Physical and Mechanical Properties. This section covers the results of density measurements on the anodes used in the pilot cell test and of studies on their mechanical properties. The mechanical properties tested included fracture strength, fracture toughness, and ductile-brittle transition temperature (DBTT). In all of this work, measurements were made on samples removed from the center of anode F1 after testing in the pilot cell. The samples were from the region of native microstructure, i.e. they did not include any of the reaction layers. Measurements on anode F1 were then compared to results on another anode (control) fabricated by CMI but not tested in the pilot cell.

The density of a sample removed from the interior of anode F1 after testing in the pilot cell was 5.67 ± 0.05 $g \cdot cm^{-3}$. This value is lower than that measured for the control anode (5.82 ± 0.01 $g \cdot cm^{-3}$) and much lower than anodes previously fabricated for studies at PNL (6.05 - 6.10 $g \cdot cm^{-3}$). The higher values for the PNL anodes are explained, at least partly, by the higher consolidation pressures used in fabrication at PNL and are also consistent with the apparently higher porosity exhibited by the pilot cell anodes (Figure 2). The drop in density as a result of pilot cell testing was not expected, however, and is probably related to the compositional changes and the presence of electrolyte components within the anode as discussed above.

Four-point bend testing was performed on rectangular bend bars (4 mm x 4 mm x 50 mm) using SiC fully-articulated bend fixtures having a lower span of 40 mm and an upper span of 20 mm. Tests were performed in air from ambient up to 1100°C at a strain rate of 1.27×10^{-4} s^{-1}. The mid-point bending deflection was measured and used to calculate stress-strain curves for each specimen. In addition, chevron-notched bend (CVN) bars were used to measure the chevron-notch fracture toughness over the same temperature range. These tests were performed at the same strain rate in four-point bending and the overall specimen dimensions were the same as the unnotched bend bars. The test temperature was measured by a Type K thermocouple inserted into the bend fixture. All data was recorded onto a computer-based data acquisition system. SEM stereo photomicrographs were taken of representative fracture surfaces above and below the DBTT of each material to characterize the mode of failure.

Measured strength and toughness were found to be low for all of the anode materials tested compared to typical cermets. Room temperature strength of 110 MPa (16 ksi) and toughness of 2.8 $MPa \cdot m^{0.5}$ were measured for the control anode. As shown in Figure 15, strength increased to 117 MPa (17 ksi) at 1000°C and then decreased above this temperature, the DBTT of the control anode material. The fracture strength of the cermet anodes was degraded as a result of pilot cell testing. As shown in Figure 15, anode F1 strength ranged from 50 MPa (7.3 ksi) at room temperature to a high of 63.3 MPa (9.2 ksi) at 350°C. The DBTT for anode F1 material was determined to be 500°C, shifted down from the control anode by 500°C.

Changes in the fracture mode accompanied the shift in the DBTT for anode F1 compared to the control anode, and the fracture mode of the control anode was different above the DBTT compared to below the DBTT.

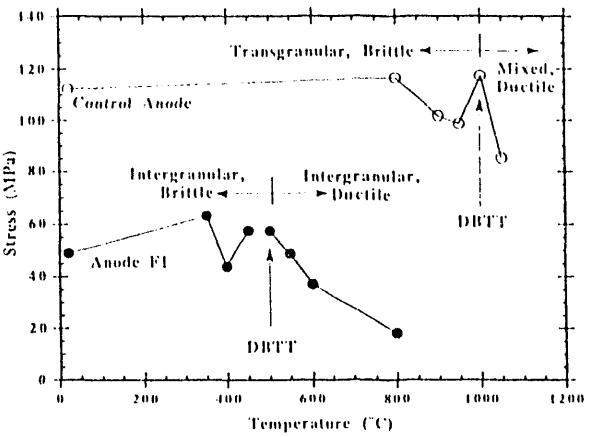

Figure 15: Variation of Fracture Stress as a Function of Temperature.

The fracture mode for the control anode was observed to be transgranular below the DBTT, but the fracture mode for anode F1 below the DBTT was intergranular. In fact, anode F1 exhibited an intergranular fracture morphology at all test temperatures. This was in contrast to the control anode which exhibited a mixed transgranular-intergranular morphology above the DBTT and was transgranular below the DBTT. Figure 16 shows the difference in fracture morphology at 20°C between the control anode (transgranular) and anode F1 (intergranular).

Interestingly, the fracture toughness behaved similar to the strength as a function of temperature for these samples. The fracture toughness was 2.5 $MPa \cdot m^{0.5}$ at 1000°C and increased to 3.7 $MPa \cdot m^{0.5}$ at 1050°C for the control anode. The values were lower for anode F1, dropping to 1.7 $MPa \cdot m^{0.5}$ at room temperature and 2.6 $MPa \cdot m^{0.5}$ at 500°C. As shown in the case of the control anode in Figure 17, the similarity in the temperature dependence of the fracture strength and fracture toughness is striking suggesting the toughness controls the strength of the material below the DBTT. The correspondence between strength and toughness was found to be similar for anode F1.

The plastic deformation of the anode material at elevated temperatures appears to be controlled by the weakest phase which is probably the distributed metallic or grain boundary phase. It is expected that the DBTT is determined by the composition and distribution of this phase. The fracture morphology change for the control anode at the DBTT is consistent with this conclusion. It is rather remarkable that the control anode can maintain brittle behavior up to 1000°C given that the metallic phase is a Cu-Ni alloy with a melting point of about 1200°C. The low toughness value implies that the ductile metallic phase is not distributed optimally for mechanical properties benefit. Apparently the alloy is too widely distributed to impact the toughness of the cermet material. In contrast, fracture toughness for cemented carbides can be as high as 18 $MPa \cdot m^{0.5}$. The fracture behavior for the anode material seems to be controlled by the cleavage strength of the oxide grains. In general, the fracture strength is controlled by fracture toughness below the DBTT for

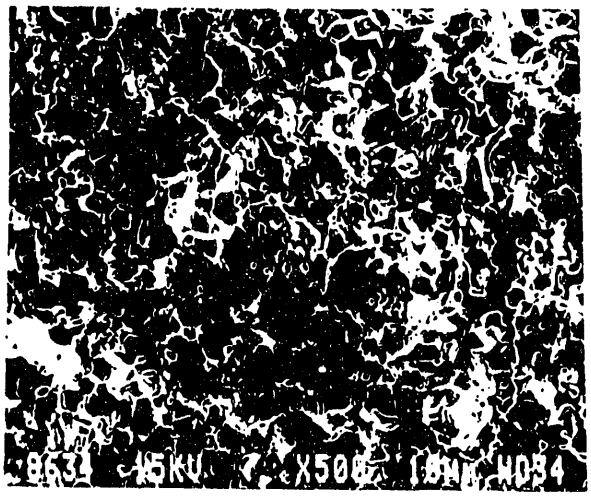

(a) Control Anode Showing Transgranular Fracture

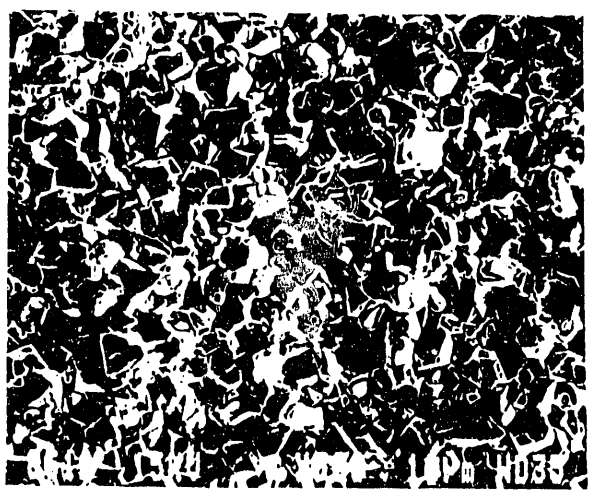

(b) Anode F1 Showing Intergranular Fracture

Figure 16: Fracture Morphology below DBTT (20°C).

these materials. The excellent correspondence between strength and toughness for the anode materials supports this conclusion.

The observed strength reduction and DBTT shift for anode F1 as a result of pilot cell testing points to degradation of the intergranular phase, perhaps due to electrolyte migration. The material no longer fails by cleavage of the oxide grains, but instead deforms at boundaries resulting in a completely intergranular fracture morphology. The changes in the fracture morphology of anode F1 compared to the control anode supports this conclusion. The presence of a Al-containing fluoride or oxyfluoride phase at the oxide grain boundaries in anode F1 material (Figure 13) suggests that this material is essentially very different from the control anode material.

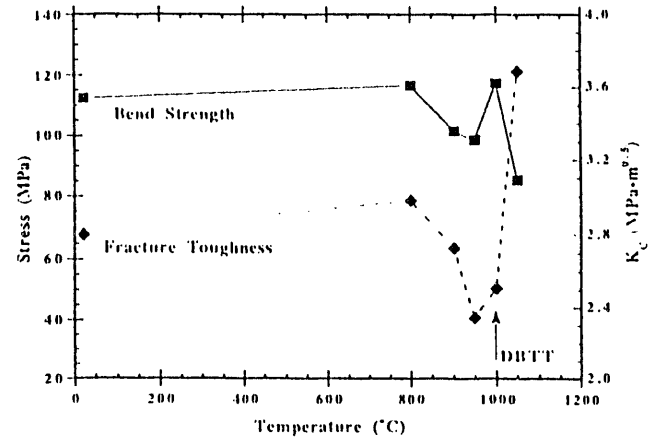

Figure 17: Toughness and Strength for Control Anode as a Function of Temperature.

A low fracture toughness, high thermal expansion coefficient, and moderately low thermal conductivity for the cermet material would also make these anodes very susceptible to thermal shock. Observed cracking during operation (5) is consistent with this and suggests that use of this material for anodes, without additional refinement of composition to increase toughness, will necessitate very delicate handling procedures.

Conclusions

Cermet anodes were tested in a pilot-scale reduction cell for up to 314 h (13.1 days). Post-test analyses of the anodes revealed changes in appearance, microstructure, composition, and physical and mechanical properties. These changes were influenced both by overall cell conditions and local conditions around each anode. Those parts of the anodes exposed to normal conditions of less than or equal to 0.5 $A \cdot cm^{-2}$ and close to alumina saturation exhibited little dimensional loss, but did show the growth of a reaction layer of significant thickness. Anodes exposed to aggressive conditions of higher current density and low alumina concentration, exhibited severe dimensional and compositional changes. Significant penetration of the electrolyte deep within the material was observed for all anodes analyzed. The penetration resulted in compositional changes even in regions above the reaction layer where the microstructure was similar to the original material. The observed changes were accompanied by a deterioration of the mechanical properties of the anodes and, as reported elsewhere in this volume (5), an increase in the amounts of anode-derived impurities in the aluminum metal.

The apparently poor performance of the anodes observed in this test can probably be attributed to one or more of the following factors: 1) the inherent limitations of the cermet material tested, 2) the differences between the composition and microstructure of the cermet material tested in the pilot cell and previous cermet material tested in the laboratory, 3) the fluctuations in cell operating conditions and, in the case of alumina concentration and current, their variance from "optimal" conditions, 4) the influence

of the large carbon anode on the voltages in the cell and possibly on anode reactions, and 5) the failure of the connector rods and the cracking of the brittle anodes, which necessitated a significant amount of electrode manipulation. Which of the above factors was most important is still uncertain at this time. Clearly, additional testing is required to determine, without ambiguity, whether the cermet material itself is in some way deficient. In any future pilot cell test on this material, it is recommended that only cermet anodes be employed (no carbon), anodes be fabricated that have microstructure and physical properties as close as possible to the anodes previously tested in the laboratory, the pilot cell test be performed using a design and procedure that minimizes fluctuations in operating conditions and more easily permits operation near alumina saturation, the pilot cell be modelled extensively before testing particularly in regards to its current and voltage characteristics, and a more durable anode design or effective heat-up strategy be used to minimize thermal shock.

Acknowledgments

The authors wish to acknowledge the other staff of the Pacific Northwest Laboratory (PNL) and the staff at the Manufacturing Technology Laboratory (MTL) of the Reynolds Metals Company (RMC) who made contributions to the pilot cell test. We are also grateful for the assistance by W. E. Haupin, program consultant, and the staff at Ceramic Magnetics, Inc., especially I. Van Dil'an and F. R. Huettig who helped direct the fabrication of the cermet anodes. Funding for this research was provided by the Office of Industrial Processes (OIP), U.S. Department of Energy (DOE). We are also grateful to M. J. McMonigle, DOE program manager, for his support during this endeavor.

References

1. J. D. Weyand, D. H. DeYoung, S. P. Ray, G. P. Tarcy, and F. W. Baker, Inert Anodes for Aluminum Smelting: Final Technical Report for the Period 1980 September 29 - 1985 September 30 (Report DOE CONS 40158-20, Alcoa Center, PA: Aluminum Company of America, 1986).

2. C. F. Windisch Jr., D. M. Strachan, N. C. Davis, L. G. Morgan, J. W. Shade, N. D. Stice, and R. L. Westerman, Inert Electrodes Program Fiscal Year 1990 Annual Report (PNL-7777, Richland, WA: Pacific Northwest Laboratory, 1991).

3. R. D. Peterson, N. E. Richards, A. T. Tabereaux, O. H. Koski, L. G. Morgan, and D. M. Strachan, "Results of 100 Hour Electrolysis Test of a Cermet Anode: Operational Results and Industry Perspective," Light Metals 1990 (Warrendale, PA: The Minerals, Metals, and Materials Society, 1990).

4. D. M. Strachan, O. H. Koski, L. G. Morgan, R. E. Westerman, R. D. Pederson, N. E. Richards, and A. T. Tabereaux, "Results from a 100-Hour Electrolysis Test of a Cermet Anode: Materials Aspects," Light Metals 1990 (Warrendale, PA: The Minerals, Metals, and Materials Society, 1990).

5. T. R. Alcorn, A. T. Tabereaux, N. E. Richards, C. F. Windisch Jr., D. M. Strachan, J. D. Gregg, and M. S. Frederick, "Operational Results of Pilot Cell Test with Cermet 'Inert' Anodes," Light Metals 1993 (Warrendale, PA: The Minerals, Metals, and Materials Society, 1993).

6. J. S. Gregg, M. S. Frederick, A. J. Vaccaro, T. R. Alcorn, A. T. Tabereaux, and N. E. Richards, "Pilot Cell Demonstration of Cerium Oxide Coated Anodes," Light Metals 1993 (Warrendale, PA: The Minerals, Metals, and Materials Society, 1993).

7. P. E. Hart, B. B. Brenden, N. C. Davis, O. H. Koski, S. C. Marschman, K. H. Pool, C. H. Schilling, C. F. Windisch Jr., and B. J. Wrona, Inert Anode/Cathode Program Fiscal Year 1986 Annual Report (PNL-6247, Richland, WA: Pacific Northwest Laboratory, 1987).

8. D. M. Strachan, S. C. Marschman, N. C. Davis, J. R. Friley, and C. H. Schilling, Fiscal Year 1988 Annual Report for the Inert Electrodes Program (PNL-7106, Richland, WA: Pacific Northwest Laboratory, 1989).

9. C. F. Windisch, Jr. and N. D. Stice, Final Report on the Characterization of the Film on Inert Anodes (PNL-7589, Richland, WA: Pacific Northwest Laboratory, 1991).

END

DATE
FILMED
5125193